# Electrochemical detection of lead ions using carbon nanotube post electrodes

<sup>1</sup>Neeraj Kumar, <sup>2</sup>Han Tran, <sup>2</sup>Vesselin N. Shanov, \*<sup>1</sup>Noe. T. Alvarez

\*Email: alvarene@ucmail.uc.edu

<sup>1</sup>Department of Chemistry, University of Cincinnati, USA-45221

<sup>2</sup>Chemical Engineering Department, University of Cincinnati, USA-45221

#### **Abstract**

1

2

4

5

6

7

8

9

10

11

12

13

14

15

16

17

18

19

20

21

22

23

Heavy metal ions above their recommended limits are highly toxic to human health. Even at low levels, contaminants such as Pb in drinking water can severely affect vulnerable population of the society. Therefore, developing rapid, effective, stable, and convenient sensors for Pb detection has gained significant attention. In this study, considering the excellent properties of carbon nanotubes (CNTs), CNT post electrodes were fabricated by embedding them in a nonconducting polymer. The CNT posts were derived from a closely packed CNT forest with a diameter of 0.3 mm containing millions of vertically aligned pillars. The highly stable CNT post electrodes were employed for the electrochemical sensing of heavy metal ions in 0.1 M citric acid. A linear range of 9.64–168.7 nM (2–35 ppb) was observed for Pb ions. Further, linear ranges of  $0.0786-7.86 \,\mu\text{M}$  (5–500 ppb) and 15.73–157.36  $\mu\text{M}$  (1000–10000 ppb) were also obtained for Cu ions. Notably, the electrode containing a single CNT post was capable of the electrochemical detection of Pb ions at the ppb level. With this electrode, the sensitivity and limit of detection were 0.5095 nA/nM and 2 nM (0.5 ppb) for Pb ions, and 24.53 μA/ppb and 41.67 nM (2.64 ppb) for Cu ions, respectively. The limit of detection for Pb ions is lower than the maximum permissible limit in drinking water set by the World Health Organization. Due the electrochemical method employed on its detection, the reported sensor can simultaneously detect Pb, Cu and Zn ions in tap water.

Keywords: carbon nanotube posts, electrochemical sensor, Pb ions, Cu ions, square wave anodic
 stripping voltammetry, electrochemical impedance spectroscopy

### 1. Introduction

26

27

28

29

30

31

32

33

34

35

36

37

38

39

40

41

42

43

44

45

46

47

48

49

50

51

52

53

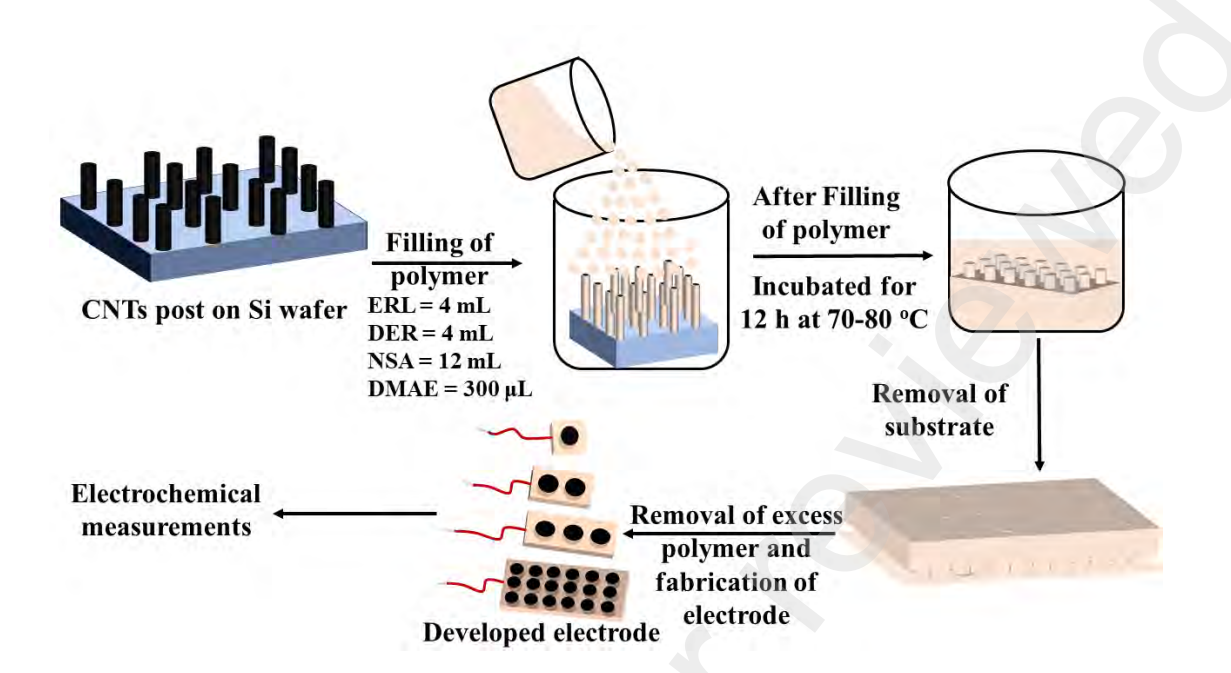
The availability of safe drinking water is gradually decreasing in both developed and developing nations as water sources is becoming contaminated with heavy metal ions such as Pb and Cu. The detection of trace heavy metals is critical to avoid their adverse effects on the environment and human health [1,2]. Heavy metals are nonbiodegradable and responsible for neurological damage and behavioral disorders in infants and children [3]. In particular, Pb is highly toxic, and even low levels can affect human organs and soft tissues, initiating cancer of the brain, kidneys, lungs, and liver [4,5]. In newborns and young infants, blood Pb concentrations of 10–15 µg/dL can result in mental and behavioral disorders. The body can absorb Pb through hand-to-mouth contact or the use of contaminated cosmetics, medicine, food, and water [1,6,7]. Pb exposure can result from smelting, mining, Pb-added gasoline, and Pb-based paint. However, the most common Pb source is the corrosion or dissolution of plumbing materials, service lines, and well components. The World Health Organization (WHO) advises that the safe limit for Pb in drinking water is 10 ppb (48.1 nM), whereas the maximum contaminant level (MCL) set by the Environmental Protection Agency (EPA) is 15 ppb (72.3 nM) [8–10]. As another toxic heavy metal, Cu can cause gastrointestinal distress as well as kidney and liver damage after long-term exposure. The MCL for Cu is 1.3 ppm (1.3 mg/L) [11,12]. Cu in drinking water can originate from the corrosion of Cu plumbing materials and service lines, such as Cu pipes and brass components. The levels of Pb and Cu ions in drinking water depend on several factors, such as water source, plumbing materials, fixtures, drinking water treatment, plumbing configuration, and water usage patterns. Thus, developing simple and reliable analytical methods for the monitoring and detection of Pb and Cu ions is important [13-15].

Several analytical and spectroscopic methods, including inductively coupled plasma mass spectrometry [16,17], inductively coupled atomic emission spectrometry [18,19] and atomic absorption spectroscopy [20], are typically employed for the selective and sensitive quantification of heavy metals. Although these methods are highly reliable, sensitive, and accurate, they require trained personnel and expensive, relatively large instruments, making them unsuitable for the in situ or on-site analysis of heavy metals [21,22]. In contrast, electrochemical methods are simple,

portable, economical, and user-friendly, thereby facilitating in-field applications and reducing the complexity of heavy metal detection [23,24].

Carbon nanotubes (CNTs) have extraordinary mechanical, thermal, and electrical properties, including a high surface area, high surface-to-volume ratio, good chemical stability, high thermal and electrical conductivity, fast electron transfer rate, wide potential window, and minimal electrode fouling. Consequently, CNTs have gained extensive attention for the development of sensors [21,25] and other applications [26–28]. Although CNTs have been widely used as modifiers of conducting electrode materials, their direct application as electrodes for detection of heavy metal ions has produced impressive detection limits. These systems include CNT towers [29], metal-catalyst-free CNTs [30], CNT nanoelectrode arrays [31], pristine single-walled CNT films [32], CNT threads [33,34], CNT nanofibers [35], and CNT microelectrodes [21]. The high proportion of edge planes in CNTs is advantageous for voltammetric analysis. The edge-plane sites have fast electron transfer rates, allowing a high sensitivity, improved signal-tonoise ratio, low overpotential, and low detection limit [31,33]. Thus, the edge-plane sites of CNTs have been employed in the fabrication of electrodes. Furthermore, the open ends of CNTs have been used as a working surface for the electrochemical detection of heavy metals.

Herein, motivated by the exceptional properties of CNTs, especially the high electric conductivity and high catalytical activity, cylindrical structures of vertically aligned CNTs (posts) were employed as electrodes for the electrochemical detection of Pb and Cu ions. Sensors were fabricated by introducing CNT posts (also called pillars or towers) into a nonconducting polymer, where the tip or edge of the CNT post was used as an electrode for heavy metal detection (**Scheme 1**). Electrodes with 1, 2, 3, or 18 CNT posts embedded within a polymer were prepared and employed for the electrochemical detection of Pd and Cu ions in water samples. Notably, the 1 CNT post electrode could detect Pb ions at nanomolar concentrations (a few ppb ~ 2 ppb). Overall, the proposed CNT post electrodes reveal great potential as electrochemical sensors for Pb ion detection.



**Scheme 1.** Fabrication of CNT post electrodes.

### 2. Materials and methods

### 2.1 Materials

Lead chloride (PbCl<sub>2</sub>), copper (std.), zinc (std.), and citric acid were purchased from Sigma Aldrich (USA). Citric acid (0.1 M) were used as a supporting electrolyte. CNT posts were synthesized using chemical vapor deposition (CVD) with ethylene as a carbon source (Wright Brothers, USA), a Al<sub>2</sub>O<sub>3</sub>/Fe/Gd catalyst (Goodfellow Corporation, USA), and Ar as a carrier gas, as reported previously by our research group [36–38]. Briefly, the CVD process was conducted in a 2-inch quartz tube reactor (ET 1000, First Nano/CVD Equipment Corporation). The growth parameters were 400 SCCM Ar, 100 SCCM H<sub>2</sub>, 75 SCCM C<sub>2</sub>H<sub>4</sub>, and 900 ppm H<sub>2</sub>O at a deposition temperature of 780 °C. To fabricate the CNT post electrodes, 1, 2, 3, or 18 CNT posts were embedded in a polymer using a low viscosity embedding kit (by Dr. Spurr) containing ERL-4221, D.E.R. 736 Epoxy Resin (DER), Nonenyl Succinic Anhydride Modified (NSA), and Dimethylaminoethanol (DMAE) monomers (Cat.# 14300, Electron Microscopy Sciences, Hatfield, PA, USA). The CNT posts were placed in a 10 mL plastic vial containing the monomer mixture (4 mL of ERL, 4 mL of DER, 12 mL of NSA, and 0.3 mL of DMAE), which was then cured by incubating for 12 h at 70–80 °C in an oven. After extraction from the plastic vial, excess polymer was removed from the top and bottom of the CNT posts by cutting with a razor blade. The bottom part was connected to

a conductive metal wire using fast-drying Ag paint and sealed with epoxy resin. All other chemicals and solvents were of analytical grade, and Milli-Q-water (18  $M\Omega$  cm) was used to prepare stock solutions.

### 2.2 Instrumentation

Electrochemical studies were conducted with a PalmSens4 electrochemical workstation (Netherlands) using a three-electrode setup. The CNT post (~0.3 mm diameter) was used as the working electrode, Pt wire as the counter electrode, and a leakless Ag/AgCl electrode as the reference electrode. Electrochemical impedance spectroscopy (EIS) experiments were performed using a 1:1 mixture of 5 mM K<sub>3</sub>[Fe(CN)<sub>6</sub>] and 0.1 M KCl over the frequency range of 100 kHz to 0.1 Hz. The surface morphologies of the CNT posts and tips of the CNT post electrodes were characterized using field emission scanning electron microscopy (FE-SEM; FEI XL30) operated at an acceleration voltage of kV. The internal structure of the CNTs was investigated using high-resolution transmission electron microscopy (HR-TEM; JOEL 2000 FX and Titan 3 80-3).

## 2.3 Electrochemical detection of metal ions

A Pb stock solution (48.2 μM) was prepared in Milli-Q water/citric acid (10 mL/0.5 mL). Citric acid (0.1 M) was used as a supporting electrolyte for electrochemical detection because of its nontoxic, environmentally friendly, and biodegradable properties. For the analysis of Pb and Cu ions, the required amount of stock solution was added to an electrochemical cell containing 0.5 mL of citric acid (0.1 M), and the total volume was made up to 10 mL using Milli-Q water. Cyclic voltammetry studies were performed using the following parameters: equilibration time, 2 s; initial potential, 0.2 mV; potential vertex 1, -0.5 V; potential vertex 2, 0.2 V; scan rate (ν), 0.05–1.0 V/s; and potential step, 0.004 V. For square wave anodic stripping voltammetry (SWASV) studies, the following conditions were applied: deposition potential, -1.2 V, deposition time, 300 s; equilibration time, 10 s; initial potential, -1.0 V; final potential, 0.3 V; frequency (f), 30 Hz; amplitude, 25 mV; and potential step, 0.004 V. After collecting each voltammogram, the CNT post electrode was regenerated by applying a potential of 800 mV for 240–400 s in blank solution.

# 3. Results and discussion

# 127 3.1 Preparation of CNT post electrodes for electrochemical sensor applications

## 128 3.1.1 Synthesis and characterization of CNT posts

Shanov's group has reported on the synthesis, processing, and characterization of vertically aligned CNT arrays for electrochemical sensor applications [29,39,40]. As highlighted in our publications [36,38], vertically grown CNTs are advantageous nanostructures, providing a huge areal density of approximately 10<sup>10</sup> CNTs per square centimeter, superlong lengths that facilitate processing, and high purity. In addition, with appropriate packaging and wiring, these arrays can serve as very sensitive electrochemical sensors owing to the involvement of a large number of CNTs in the sensing process. To achieve centimeter-long CNT arrays, our team has employed a patented catalyst containing Fe and Gd, as described previously [36–38,41,42]. Vertically aligned multiwalled CNT arrays with a record length (21.7 mm) were synthesized using a thermal CVD process [36,37,41]. The catalyst lifetime was maintained for 790 min under optimized experimental conditions. The growth kinetics of the super-long CNTs was investigated using realtime photography under different growth conditions [41]. Optimization of the ratio of ethylene and H<sub>2</sub> as well as the water and ethylene concentrations led to a prolonged catalyst lifetime [36,37]. Details about the catalyst preparation process, CVD synthesis conditions, and characterization of the vertically aligned CNT arrays and posts can be found in our previous publications [36,37]. In short, 4-inch Si wafers with a 500 nm thick thermal oxide layer were used as substrates. On the oxide layer, a catalyst structure consisting of 6 nm of Al<sub>2</sub>O<sub>3</sub> and 1.5 nm of a Fe/Gd alloy (80/20%) was deposited using an e-beam through a removable stainless-steel shadow mask. The mask had openings with diameters of 0.1–1 mm, which provided control over the diameter of the catalyst islands on the substrate and thus the diameter of the grown CNT posts. The increased growth length achieved during the CVD process used to produce vertically aligned CNTs was due to two factors. First, the presence of 0.1 vol% water vapor in the gas mixture prolonged the catalyst lifetime by removing amorphous carbon from the catalyst surface. Second, the Gd component in the Fe-based catalyst alloy controlled the carbon flux reaching the catalyst, thereby preventing inactivation [36,37,41]. The combination of these factors enabled a linear growth rate of approximately 50 µm/min and the growth of centimeter-long CNT arrays and posts. Despite the long growth time and CNT length, the CNTs grew vertically without interruption until the catalyst was deactivated.

129

130

131

132

133

134

135

136

137

138

139

140

141

142

143

144

145

146

147

148

149

150

151

152

153

154

155

156

157

158

159

The morphologies of the vertically aligned CNT arrays and posts were investigated using FE-SEM, and the internal structure of the CNTs was observed using HR-TEM (Fig. 1). Because of stress accumulation during the multi-hour growth of centimeter-long CNT posts, the

straightness is slightly compromised, and some bent CNT posts are produced. When the growth period is shorter, straight arrays of vertically aligned CNT posts are easily achieved, as shown in **Fig. S1A,B**. However, shorter posts are more difficult to process as electrochemical sensors.

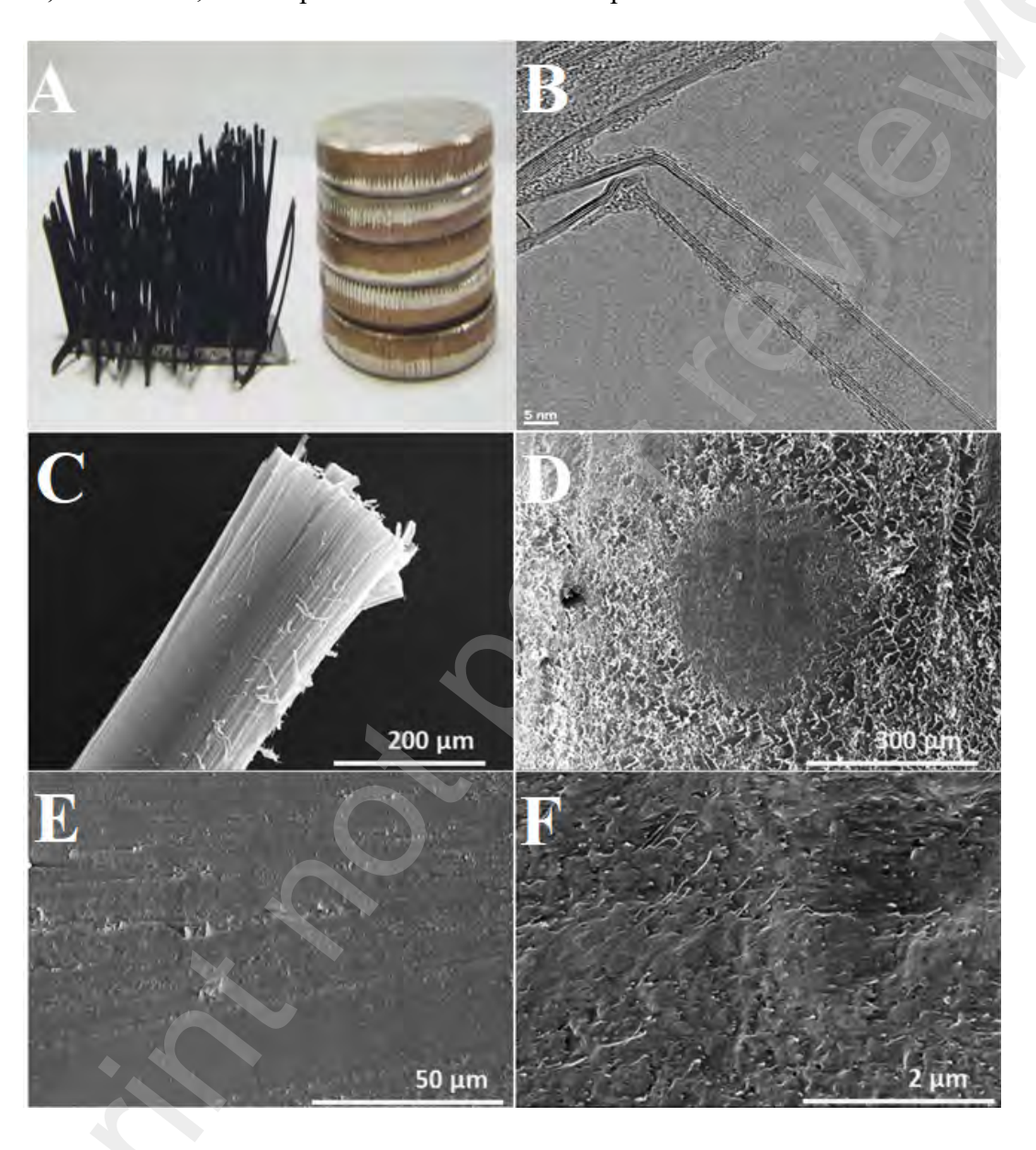


**Fig. 1.** (A) Optical image of CNT posts (8 mm length, 0.3 mm diameter, 0.3 mm post spacing) grown on the  $Al_2O_3/Fe/Gd$  catalyst in 10 h. (B) HR-TEM image of an individual CNT from a CNT post, revealing a multiwall structure without any incorporation of the metal catalyst. (C) FE-SEM image of a single CNT post. (D) cross-sectional FE-SEM image of an open-ended CNT post embedded in the polymer. (E,F) high-magnification FE-SEM images of an open-ended CNT post electrode.

# 3.1.2 Fabrication and characterization of CNT post electrodes

The vertically aligned CNT array grown on a Si wafter consisted of CNT posts with a diameter of 0.3 nm and length of ~8 mm, with each CNT post containing millions of vertically aligned CNTs [43]. These CNTs are held together via van der Waals and capillary forces, which leads to stability, bundling, and strengthening within the CNT array [44]. The obtained CNT posts were directly used without any pretreatment to fabricate CNT post electrodes. Individual CNT posts were separated from the array using tweezers. The FE-SEM image of a CNT post (~0.3 mm diameter) is shown in **Fig. 1C**. The desired number of CNT posts (1, 2, 3, or 18) were immersed in the monomer mixture (ERL, DER, NSA, and DMAE), which was then cured for 12 h at 70–80 °C. After removing excess polymer from the top and bottom of the CNT post, the bottom was connected to a conductive metal wire using Ag paint and sealed with epoxy resin for electrical insulation (**Scheme 1**). The other side of the CNT post, which contained open-ended CNTs, was used as a working electrode for the electrochemical detection of Pb and Cu ions. **Fig. 1D** shows the cross-section of a CNT post embedded in the polymer, and **Fig. 1E,F** shows FE-SEM images of the CNT post electrode at different magnifications.

The CNT post electrodes were further characterized by recording the electrochemical response in a solution containing 5 mM Ru(NH<sub>3</sub>)<sub>6</sub>Cl<sub>3</sub> (prepared in 50 mM KCl). Cyclic voltammograms were recorded at a scan rate of 50 mV/s using the 1, 2, 3, and 18 CNT post electrodes (**Fig. 2A**). The surface of the developed CNT post electrode was characterized using EIS, a well-known method for investigating the charge-transfer resistance ( $R_{ct}$ ), which can be calculated from the Nyquist plot. Using [Fe(CN)<sub>6</sub>]<sup>3-/4-</sup> as a redox probe, EIS was used to investigate the effect of the number of CNT posts (1, 2, 3, or 18) on the electrochemical behavior (**Fig. 2B**). The  $R_{ct}$  values calculated by fitting the Randles circuit were 1111, 941.1, 629.4, and 35.47 k $\Omega$  for the 1, 2, 3, and 18 CNT post electrodes, respectively. The significant reduction in  $R_{ct}$  observed for the 18 CNT post electrode relative to that for the 1 CNT post electrode demonstrates that the electrode conductivity improves with the number of posts.

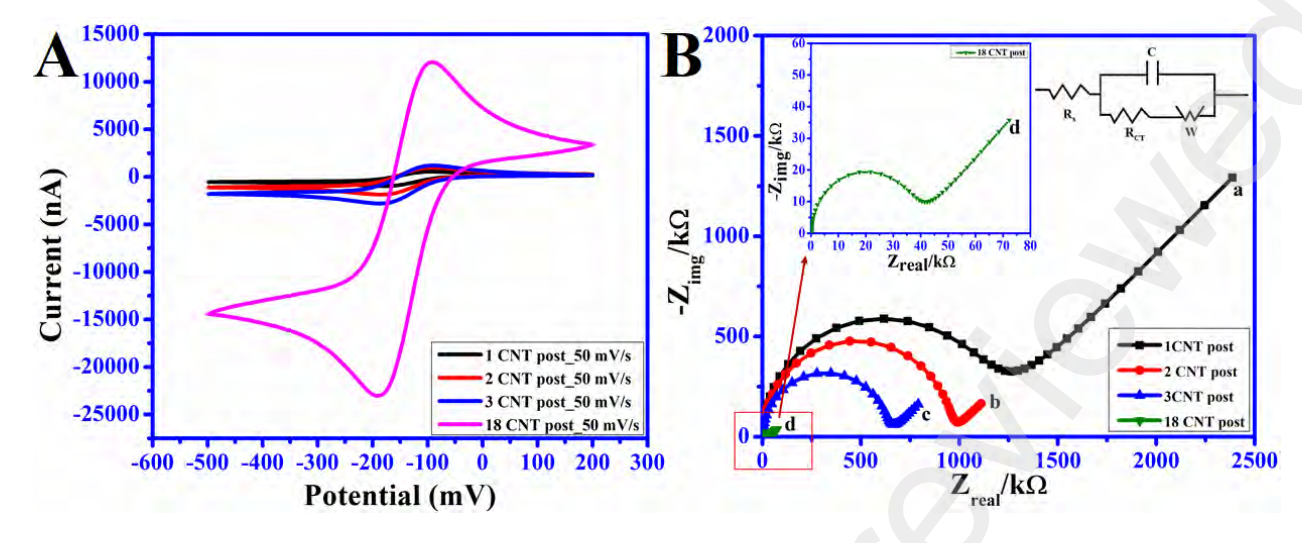


**Fig. 2.** (A) Comparison of the cyclic voltammograms of 5 mM Ru(NH<sub>3</sub>)<sub>6</sub>Cl<sub>3</sub> in 50 mM KCl at a scan rate of 50 mV/s collected using the 1, 2, 3, and 18 CNT post electrodes. (B) Typical Nyquist plots for the (a) 1, (b) 2, (c) 3, and (d) 18 CNT post electrodes in a 1:1 mixture of 0.1 M KCl and 5 mM K<sub>3</sub>[Fe(CN)<sub>6</sub>] within the frequency range of 100 kHz to 0.1 Hz. The inset shows the Randles circuit.

# 3.2 Cyclic voltammetry

To investigate the electrochemical behavior of the open-ended CNT post electrodes, cyclic voltammograms were recorded in the 5 mM Ru(NH<sub>3</sub>)<sub>6</sub>Cl<sub>3</sub> solution (prepared in 50 mM KCl) using the 1, 2, 3, and 18 CNT post electrodes at scan rates of 5–1000 mV/s (**Fig. 3A–D**). With Ru(NH<sub>3</sub>)<sub>6</sub><sup>3+/2+</sup> as the redox probe, well-defined anodic and cathodic peak current responses were observed. The current intensity increased significantly as the number of posts increased and as the scan rate increased. As shown in **Fig. 3A'–D'**, linear relationships were found between the peak current signal and the square root of the scan rate ( $v^{1/2}$ ), demonstrating the reversible reaction of the redox probe at the CNT post electrode–electrolyte interface. The change in the peak current ( $i_p$ ) with  $v^{1/2}$  can be expressed as follows:

For the 1 CNT post electrode,

$$i_{\text{pa}} = 3640.2v^{1/2} + 141.46, R^2 = 0.999$$

$$i_{\rm pc} = -3866.8v^{1/2} - 124.41, \, R^2 = 0.999$$

For the 2 CNT post electrode,

218 
$$i_{pa} = 5784.2v^{1/2} + 509.7, R^2 = 0.999$$

$$i_{pc} = -6432.8v^{1/2} - 449.31, R^2 = 0.999$$

For the 3 CNT post electrode,

$$i_{\text{pa}} = 7896.3v^{1/2} + 838.57, \,\mathbf{R}^2 = 0.999$$

$$i_{pc} = -8928.4v^{1/2} - 750.93, R^2 = 0.999$$

For the 18 CNT post electrode,

$$i_{pa} = 67661v^{1/2} + 6745.8, R^2 = 0.998$$

$$i_{\rm pc} = -76042v^{1/2} - 6132.7, \, R^2 = 0.999$$

where  $R^2$  is the regression coefficient,  $i_{pc}$  is the cathodic peak current (nA),  $i_{pa}$  is the anodic peak current (nA), and v is the scan rate (mV/s). These linear relationships indicate that electron transfer at the CNT post electrode surface was a diffusion-controlled process.

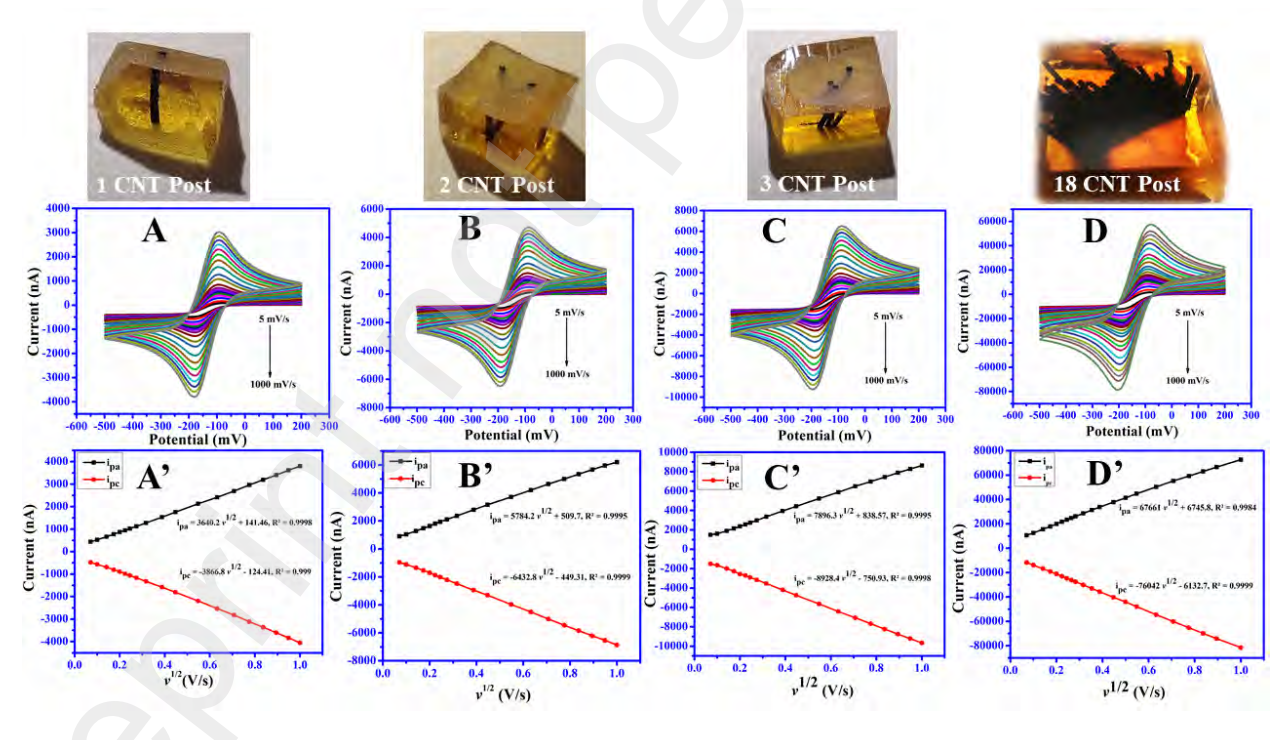


**Fig. 3.** Cyclic voltammograms of the (A) 1, (B) 2, (C), and (D) 18 CNT post electrodes at various scan rates (5–1000 mV/s) in 0.05 M KCl containing 5 mM Ru(NH<sub>3</sub>)<sub>6</sub>Cl<sub>3</sub>, and (A'–D') corresponding linear plots between the anodic or cathodic peak current and the square root of the scan rate.

## 3.2 Parameter optimization for Pb ion detection

## 3.2.1 Effect of deposition potential and applied frequency

For electrochemical sensors based on SWASV, the deposition potential and frequency play important roles in the limit of detection (LOD) and sensitivity. Therefore, the effects of these parameters were investigated using the 1 CNT post electrode at a fixed concentration of 24.1 nM Pb ions in 0.1 M citric acid. As shown in Fig. S2A,B, the peak current increased as the deposition potential increased from -1.4 to -1.0 V. The highest peak current was observed at -1.3 V and was similar to the peak current at -1.2 V. Beyond this potential, the peak current began to decrease. This decrease occurred because a more negative deposition potential induces the hydrogen evolution reaction on the electrode surface, which reduces the amount of available active sites [45,46]. Therefore, -1.2 V was chosen as the optimal deposition potential for metal ions. Additionally, the peak current of Pb ions increased upon increasing the applied frequency from 10 to 30 Hz (Fig. S2C,D). Therefore, the optimal frequency of 30 Hz was used for further analysis of heavy metal ions.

# 3.2.2 Effect of the number of CNT posts

To investigate the influence of the number of CNT posts on the electrochemical behavior, SWASV tests were performed using a Pb ion concentration of 24.1 nM in 0.1 M citric acid with the 1, 2, 3, and 18 CNT post electrodes (**Fig. 4**). The lowest electrochemical signal (~3.75 nA at -470 mV) was obtained with the 1 CNT post electrode (**Fig. 4A**). Upon increasing the number of CNT posts from 1 to 2, a small change in the current response was observed (**Fig. 4B**), whereas with 3 CNT posts, the current response increased to ~9 nA (**Fig. 4C**). With the 18 CNT post electrode (**Fig. 4D**), the current response increased significantly to ~110 nA, which is extremely high when compared to that with the 1 CNT post electrode. Although the current increased significantly as the number of CNT posts increased, the peak potential remained constant. However, as the number of CNT posts increased, the background current also increased. Therefore, the 1 CNT post electrode was selected for the electrochemical detection of Pb ions.

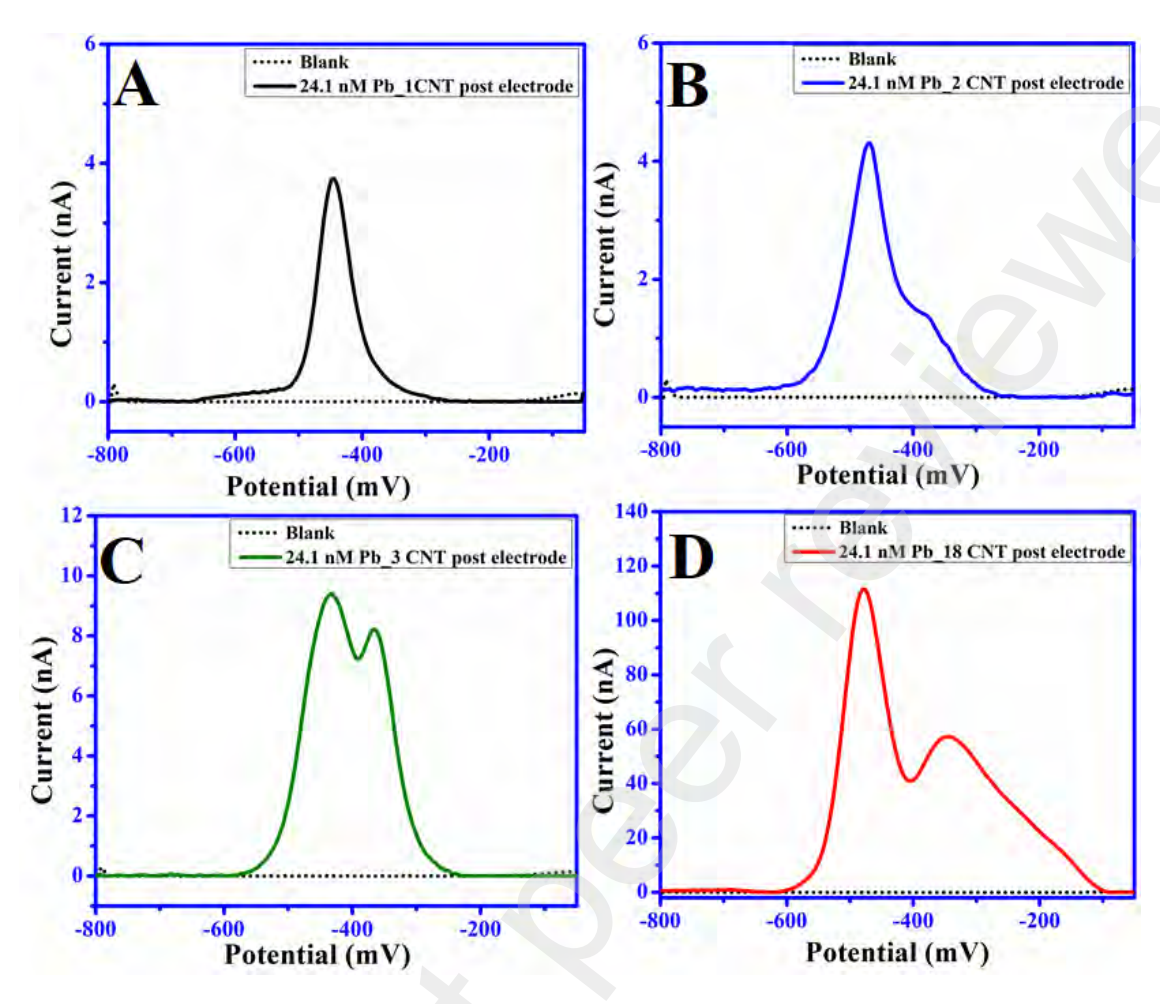


**Fig. 4.** Comparison of square wave anodic stripping voltammograms for 24.1 nM Pb ions in 0.1 M citric acid collected using the (A) 1, (B) 2, (C) 3, and (D) 18 CNT post electrodes. The dotted lines showed the blank response in 0.1 M citric acid for each CNT post electrode.

# 3.2.3 Effect of deoxygenation

To investigate the effect of deoxygenation on the detection of Pb ions, SWASV responses before and after deoxygenation of a 24.1 nM Pb ion solution were recorded using the 1 CNT post electrode (Fig. S3). Fig. S3A shows the response before background subtraction, whereas Fig. S3B shows the response after background subtraction for 24.1 nM Pb ions. A small peak was observed at  $\sim$ 518 mV when oxygen was present in the 24.1 nM Pb ion solution (blue curve). After purging with N<sub>2</sub> for 5 min to remove dissolved oxygen, a sharp peak appeared at  $\sim$ 470 mV (red curve). These results demonstrate that dissolved oxygen interferes with the electrochemical detection of Pb ions using the CNT post electrodes.

## 3.3 Pb and Cu ion detection in Milli-Q and tap water

### 3.3.1 Pb and Cu ion detection in Milli-Q-water

The 1 CNT post electrode was applied for the detection of Pb and Cu ions simultaneously presented in the tested sample by using SWASV (**Fig. 5**). A constant deposition potential of -1.2 V for 300 s was used for all stripping analyses. The detection of Pb ions at concentrations of 9.64–168.7 nM (2–35 ppb) was investigated. As shown in **Fig. 5A**, a sharp oxidation peak was observed at approximately -470 mV vs. Ag/AgCl for the oxidation of Pb ions on the CNT post electrode surface. A good linear relationship was found between the peak current and Pb concentration (inset, **Fig. 5A**). The linear regression equation is as follows:

$$i_p = 0.5095[C, 9.64-168.7 \text{ nM}] - 10.978, R^2 = 0.956$$

The LOD was calculated using the formula  $3\sigma/b$ , where  $\sigma$  is the standard deviation of the blank response (S/N =3) and b is the slope of the calibration plot. The sensitivity and LOD of the developed sensor for Pb ions were found to be 0.5095 nM/nA and 2.0 nM (~0.5 ppb), respectively.

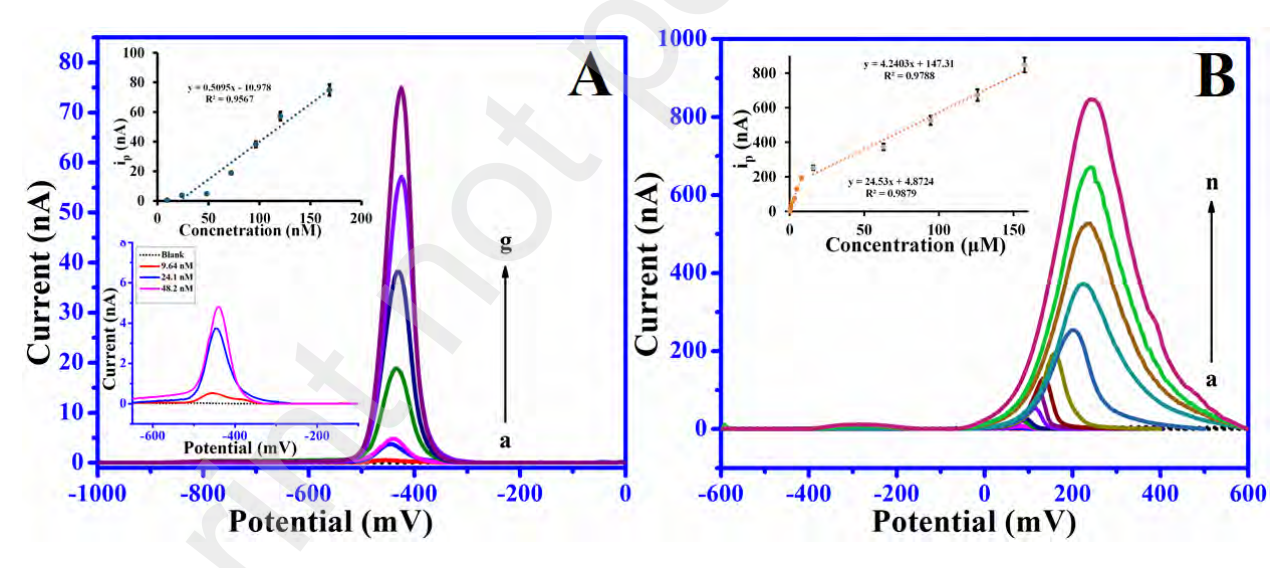


**Fig. 5.** A) SWASV response on the 1 CNT post electrode in 0.1 M citric acid containing Pb ion concentrations of (a) 9.64, (b) 24.1, (c) 48.2, (d) 72.3, (e) 96.4, (f) 120.5, and (g) 168.7 nM. Inset: Calibration plot for current response versus Pb ion concentration. B) SWASV response on the 1 CNT post electrode in 0.1 M citric acid containing Cu ion concentrations of (a) 0.0786, (b) 0.157, (c) 0.314, (d) 0.472, (e) 0.786, (f) 1.57, (g) 3.15, (h) 4.72, (i) 7.86, (j) 15.73, (k) 62.94, (l) 94.42, (m) 125.90, and (n) 157.36 μM. Inset: Calibration plot for current response versus Cu ion concentrations.

The effect of the Cu ion concentrations on the electrochemical response of the 1 CNT post electrode was also investigated. **Fig. 5B** shows the SWASV responses recorded at various Cu ion concentrations. The calibration plot for Cu ion detection exhibited two different linear ranges at 0.0786-7.86 µM (5–500 ppb) and 15.73–157.36 µM (1000–10000 ppb) (inset, **Fig. 5B**). It has been found that beyond a certain Cu ion concentration, the peak current does not increase linearly with increase in the concentration. This behavior can be the attributed to the saturation of active sites on CNT post electrode at higher concentrations, resulting the two linear ranges [21,47]. During Cu ion detection, at higher concentrations, the electrode was cleaned for a longer time (240–400 s at 0.8 V). The linear relationships between the peak current and Cu ion concentration can be expressed as follows:

307 
$$i_p = 24.53[C, 0.0786-7.86 \mu M] + 4.8724, R^2 = 0.988$$

308 
$$i_p = 4.2403[C, 15.73-157.36 \mu M] + 147.31, R^2 = 0.978$$

where R<sup>2</sup> is the correlation coefficient. The sensitivity and LOD of the developed 1 CNT post sensor for Cu ion detection were 24.528 μM/nA and 41.67 nM (2.64 ppb), respectively.

### 3.3.2 Pb ion detection in tap water

In the USA, drinking water supplies meet the WHO and EPA standards, however, the EPA has reported the release of heavy metals from pipelines after supply [21,48]. The presence of dissolved impurities, inorganic solids, and heavy metals in drinking water can alter the electrochemical response or applicability of sensors. Therefore, the detection of Pb ions in drinking water was examined to verify the suitability of the CNT post electrodes for application in real water samples. The 1 CNT post electrode was applied to detect Pb ions added to a tap water sample collected from Rieveschl Hall, University of Cincinnati, OH, on May 7, 2024 (hot tap). The concentration of metal ions in tap water samples can vary depending on the materials used in making the pipelines. The applied preconcentration potential (-1.2 V for 300 s) was sufficient to reduce metal ions (e.g., Cu, Pb, and Zn). To ensure sufficient conductivity of the tap water sample, 0.1 M citric acid (0.5 mL/10 mL) was added. SWAS voltammograms were recorded for various concentrations of Pb ions (24.1–482 nM; 5–100 ppb). Before recording the stripping response with Pb ions, the response was recorded in a blank solution (0.5 mL citric acid + 9.5 mL tap water). In the blank sample, a

sharp peak was observed at ~50 mV corresponding to Cu ions (dotted line, **Fig. 6A, B**). At lower concentrations of added Pb ions (24.1–48.2 nM), a well-defined Pb ion peak was observed at approximately -329.3 mV (**Fig. 6B**). However, at high concentrations (96.4–482 nM), an additional peak for Pb ions appeared -457.7 mV), as shown in **Fig. 6A**. Linear response curves were obtained in the Pb ion concentration ranges of (i) 24.1–482 nM at -329.3 mV and (ii) 96.4–482 nM at -457.7 mV, as given by the following equations:

331 
$$i_p = 0.0171[C, 24.1-482 \text{ nM}] + 0.9186, R^2 = 0.991$$
  
332  $i_p = 0.3124[C, 96.4-482 \text{ nM}] - 31.303, R^2 = 0.975$ 

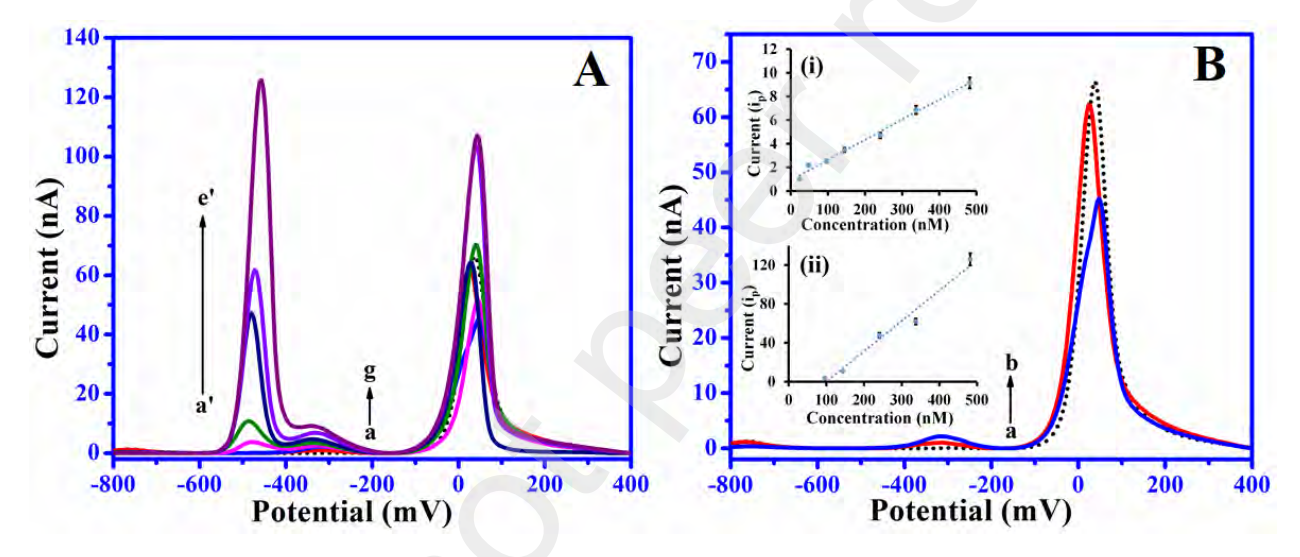


**Fig. 6.** Square wave anodic stripping voltammograms of tap water samples containing 0.1 M citric acid with added Pb concentrations of (A) 24.1–482 nM and (B) 24.1–48.2 nM. The dotted lines show the response of the blank solution.

## 3.4 Interference study

An interference study was performed to examine the effect of potential interfering metal ions on the detection of the target metal ions. The performance of the developed 1 CNT post electrode was evaluated at a constant Pb ion concentration of 24.1 nM (5 ppb) while increasing the concentrations of Cu and Zn ions (**Fig. 7**). No significant interference was observed when the Cu ion concentration was up to 10-times higher than that of Pb (**Fig. 7A**). However, the Pb ion current response of the electrode decreased by 50% in the presence of 100 ppb Cu ions (**Fig. 7B**). Furthermore, at a higher

Cu ion concentration of 200 ppb, the Pb ion peak shifted toward a lower potential. With Zn ions, no interference was observed up to 20 ppb. At higher Zn ion concentrations, the Pb ion current response decreased as the concentration of Zn ions increased, and a small shift in the Pb ion oxidation potential occurred (Fig. 7C).

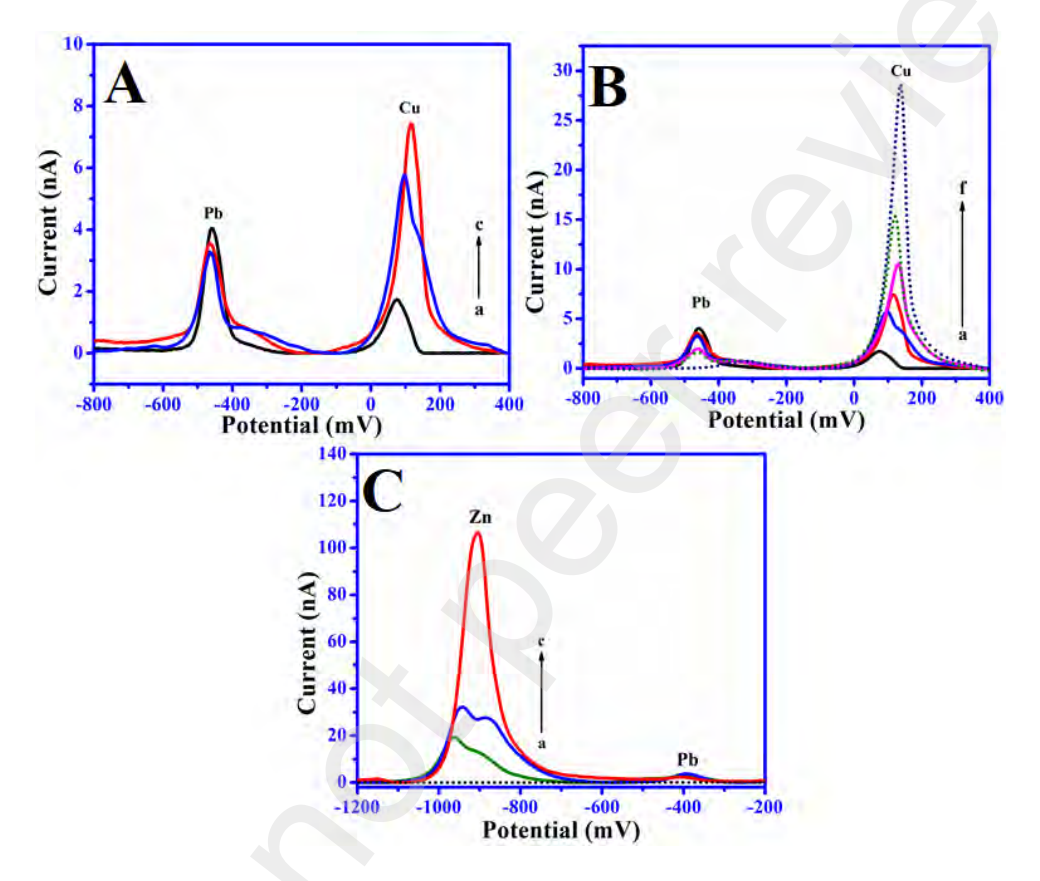


**Fig. 7.** Square wave anodic stripping voltammograms of solutions containing (A,B) 24.1 nM Pb ions with (a) 0.314, (b) 0.472, (c) 0.786, (d) 0.944 ppb, (e) 1.57 ppb, and (f) 3.15  $\mu$ M Cu ions; (C) 24.1 nM Pb ions with (a) 0.306, (b) 0.764, and (c) 3.06  $\mu$ M Zn ions. The dotted lines show the response of the blank solution.

## 3.5 Stability of CNT post electrode

To fabricate the CNT post electrode, Ag paint was applied to form a connection between the CNT post and a Cu wire. Therefore, the stability of the CNT post electrode was tested in terms of Ag paint leakage. Given the high purity of the CNT posts, determining whether Ag leakage affects the electrochemical response of the CNT post electrode during prolonged use is critical. To evaluate the stability, the CNT post electrode was immersed in a blank solution containing 9.5 mL of Milli-

Q water and 0.5 mL of 0.1 M citric acid for an extended period. The electrochemical response was recorded at regular time intervals to monitor Ag leakage or stability. No peak corresponding to Ag leakage was observed up to 7 days of testing. This study also found that the pores of the CNT posts were filled by the polymer, which is advantageous for preparing commercial electrodes. The polymer curing process helped minimize the porosity of the CNT posts, and also played a significant role in densifying the CNTs within the posts.

### 4. Conclusion

Based on the unique properties of vertically aligned CNTs, CNT post electrodes were developed for the electrochemical detection of Pb and Cu ions. The effect of the CNT posts was initially investigated using the Ru<sup>3+/2+</sup> redox probe, and the electrochemical responses for Pb ions were successfully compared for electrodes containing 1, 2, 3, and 18 CNT posts. The CNT posts and CNT post electrodes were characterized using FE-SEM, EIS, and SWASV. The SWASV technique was employed to detect Pb and Cu ions in Milli-Q and tap water. In Milli-Q water, good linear ranges were observed with the 1 CNT post electrode (9.64–168.7 nM for Pb ions, and 0.0786-7.86  $\mu$ M and 15.73-157.36  $\mu$ M for Cu ions). The LOD of the sensor was less than 1 ppb for Pb ions and 3 ppb for Cu ions. Additionally, Pb ions were successfully detected in tap water samples at concentrations of 24.1–482 nM. The potential interfering metals Zn (0.306  $\mu$ M) and Cu (0.786  $\mu$ M) did not interfere with the detection of Pb ions. It has been shown that the 1 CNT post electrode could be applied for the detection of Pb ions at ppb levels. Moreover, by using multiple CNT posts, the electrochemical response for Pb ion detection could be improved. The obtained results demonstrate that CNT post electrodes are effective for the electrochemical sensing of Pb ions in real water samples, as verified by using tap water.

### Acknowledgment

This work was supported by NSF PFI-RP grant number 2016484.

## 392 References

- W. Kang, X. Pei, C.A. Rusinek, A. Bange, E.N. Haynes, W.R. Heineman, I. Papautsky,
   Determination of Lead with a Copper-Based Electrochemical Sensor, Anal. Chem. 89 (2017)
   3345–3352. https://doi.org/10.1021/acs.analchem.6b03894.
- 396 [2] A.U. Alam, M.M.R. Howlader, N.-X. Hu, M.J. Deen, Electrochemical sensing of lead in drinking water using β-cyclodextrin-modified MWCNTs, Sens. Actuators B Chem. 296
   398 (2019) 126632. https://doi.org/10.1016/j.snb.2019.126632.
- Y.Y. Heng, I. Asad, B. Coleman, L. Menard, S. Benki-Nugent, F. Hussein Were, C.J. Karr,
   M.S. McHenry, Heavy metals and neurodevelopment of children in low and middle-income countries: A systematic review, PLOS ONE 17 (2022) e0265536.
   https://doi.org/10.1371/journal.pone.0265536.
- 403 [4] M.S. Collin, S.K. Venkatraman, N. Vijayakumar, V. Kanimozhi, S.M. Arbaaz, R.G.S.
   404 Stacey, J. Anusha, R. Choudhary, V. Lvov, G.I. Tovar, F. Senatov, S. Koppala, S.
   405 Swamiappan, Bioaccumulation of lead (Pb) and its effects on human: A review, J. Hazard.
   406 Mater. Adv. 7 (2022) 100094. https://doi.org/10.1016/j.hazadv.2022.100094.
- 407 [5] A. Rădulescu, S. Lundgren, A pharmacokinetic model of lead absorption and calcium competitive dynamics, Sci. Rep. 9 (2019) 14225. https://doi.org/10.1038/s41598-019-50654-409 7.
- 410 [6] Limiting Lead in Lipstick and Other Cosmetics | FDA, (n.d.).
  411 https://www.fda.gov/cosmetics/cosmetic-products/limiting-lead-lipstick-and-other412 cosmetics (accessed May 15, 2024).
- L.W. Stanek, J. Xue, C.R. Lay, E.C. Helm, M. Schock, D.A. Lytle, T.F. Speth, V.G.
   Zartarian, Modeled Impacts of Drinking Water Pb Reduction Scenarios on Children's
   Exposures and Blood Lead Levels, Environ. Sci. Technol. 54 (2020) 9474–9482.
   https://doi.org/10.1021/acs.est.0c00479.
- 417 [8] G.R. Dangel, A. Huseinov, A. Hoque, C.P. Nawarathne, E. Dominique, N.T. Alvarez, Electrochemical Quantification of Lead Scale Particulates in Drinking Water, ACS EST Water 4 (2024) 1371–1380. https://doi.org/10.1021/acsestwater.3c00519.
- 420 [9] A. Huseinov, A. Hoque, K.A. Ruble, B.J. Dee, N.T. Alvarez, Reagentless Dissolution and Quantification of Particulate Lead in Tap Water via Membrane Electrolysis, Anal. Chem. 95 (2023) 9297–9303. https://doi.org/10.1021/acs.analchem.3c01201.
- 423 [10] C.E. Rahm, P. Gupta, V.K. Gupta, A. Huseinov, B. Griesmer, N.T. Alvarez, Impact of 424 physical and chemical parameters on square wave anodic stripping voltammetry for trace 425 Pb2+ detection The Analyst 147 (2022)3542-3557. in water, 426 https://doi.org/10.1039/D2AN00724J.
- 427 [11] W.-C. Lin, Z. Li, M.A. Burns, A Drinking Water Sensor for Lead and Other Heavy Metals,
   428 Anal. Chem. 89 (2017) 8748–8756. https://doi.org/10.1021/acs.analchem.7b00843.
- 429 [12] O. US EPA, National Primary Drinking Water Regulations, (2015).
   430 https://www.epa.gov/ground-water-and-drinking-water/national-primary-drinking-water-regulations (accessed May 12, 2024).
- [13] K.D. Bradham, C.M. Nelson, T.D. Sowers, D.A. Lytle, J. Tully, M.R. Schock, K. Li, M.D. Blackmon, K. Kovalcik, D. Cox, G. Dewalt, W. Friedman, E.A. Pinzer, P.J. Ashley, A national survey of lead and other metal(loids) in residential drinking water in the United States, J. Expo. Sci. Environ. Epidemiol. 33 (2023) 160–167. https://doi.org/10.1038/s41370-022-00461-6.

- 437 [14] Proposed Lead and Copper Rule Improvements | US EPA, (n.d.).
  438 https://www.epa.gov/ground-water-and-drinking-water/proposed-lead-and-copper-ruleimprovements (accessed May 15, 2024).
- [15] J.M. Gibson, A. Desclos, J. Harrington, S.P. McElmurry, R. Mulhern, Effect of Community
   Water Service on Lead in Drinking Water in an Environmental Justice Community, Environ.
   Sci. Technol. 58 (2024) 1441–1451. https://doi.org/10.1021/acs.est.3c01341.
- 443 [16] M. Jin, H. Yuan, B. Liu, J. Peng, L. Xu, D. Yang, Review of the distribution and detection methods of heavy metals in the environment, Anal. Methods 12 (2020) 5747–5766. https://doi.org/10.1039/D0AY01577F.
- [17] S.M. Harmon, J. Tully, M.K. DeSantis, M.R. Schock, S. Triantafyllidou, D.A. Lytle, A
   holistic approach to lead pipe scale analysis: Importance, methodology, and limitations,
   AWWA Water Sci. 4 (2022) e1278. https://doi.org/10.1002/aws2.1278.

449

450

451

452

453

454

455

456

457

458

459

460

461

462

463

464

465

- [18] Z. Herrero Fernández, J.R. Estevez Álvarez, A. Montero Álvarez, O. Muñiz Ugarte, I. Pupo González, M. Rodríguez González, J.A. Dos Santos Júnior, M.B.C.F. Bezerra, O.P. Dos Santos Junior, Metal contaminants in rice from Cuba analyzed by ICP-MS, ICP-AES and CVAAS, Food Addit. Contam. Part B 14 (2021) 59–65. https://doi.org/10.1080/19393210.2020.1870576.
- [19] D.P. Mokoena, S.V. Mngadi, M. Sihlahla, M.K. Dimpe, P.N. Nomngongo, Development of a Rapid and Simple Digestion Method of Freshwater Sediments for As, Cd, Cr, Cu, Pb, Fe, and Zn Determination by Inductively Coupled Plasma-Optical Emission Spectroscopy (ICP-OES): An Evaluation of Dilute Nitric Acid, Soil Sediment Contam. Int. J. 28 (2019) 323–333. https://doi.org/10.1080/15320383.2019.1575334.
- [20] R. Manjusha, R. Shekhar, S.J. Kumar, Ultrasound-assisted extraction of Pb, Cd, Cr, Mn, Fe, Cu, Zn from edible oils with tetramethylammonium hydroxide and EDTA followed by determination using graphite furnace atomic absorption spectrometer, Food Chem. 294 (2019) 384–389. https://doi.org/10.1016/j.foodchem.2019.04.104.
- [21] P. Gupta, C.E. Rahm, D. Jiang, V.K. Gupta, W.R. Heineman, G. Justin, N.T. Alvarez, Parts per trillion detection of heavy metals in as-is tap water using carbon nanotube microelectrodes, Anal. Chim. Acta 1155 (2021) 338353. https://doi.org/10.1016/j.aca.2021.338353.
- 467 [22] G. Aragay, J. Pons, A. Merkoçi, Recent Trends in Macro-, Micro-, and Nanomaterial-Based 468 Tools and Strategies for Heavy-Metal Detection, Chem. Rev. 111 (2011) 3433–3458. 469 https://doi.org/10.1021/cr100383r.
- [23] S.F. Sulthana, U.M. Iqbal, S.B. Suseela, R. Anbazhagan, R. Chinthaginjala, D. Chitathuru, I.
   Ahmad, T. Kim, Electrochemical Sensors for Heavy Metal Ion Detection in Aqueous
   Medium: A Systematic Review, ACS Omega (2024) acsomega.4c00933.
   https://doi.org/10.1021/acsomega.4c00933.
- 474 [24] R. Ding, Y.H. Cheong, A. Ahamed, G. Lisak, Heavy Metals Detection with Paper-Based 475 Electrochemical Sensors, Anal. Chem. 93 (2021) 1880–1888. 476 https://doi.org/10.1021/acs.analchem.0c04247.
- [25] N. Kumar, P.C. Thapliyal, Graphene and carbon nanotube-based sensors, in: Sens. -Gener.
   Electron. Syst. Technol., 1st ed., CRC Press, 2023: pp. 193–224.
- [26] K. Komatsubara, H. Suzuki, H. Inoue, M. Kishibuchi, S. Takahashi, T. Marui, S. Umezawa,
  T. Nakagawa, K. Nasu, M. Maetani, Y. Tanaka, M. Yamada, T. Nishikawa, Y. Yamashita,
  M. Hada, Y. Hayashi, Highly Oriented Carbon Nanotube Supercapacitors, ACS Appl. Nano
  Mater. 5 (2022) 1521–1532. https://doi.org/10.1021/acsanm.1c04236.

- 483 [27] D. Tasis, N. Tagmatarchis, A. Bianco, M. Prato, Chemistry of Carbon Nanotubes, Chem. Rev. 106 (2006) 1105–1136. https://doi.org/10.1021/cr050569o.
- 485 [28] N. Kumar, Rosy, R.N. Goyal, Palladium nano particles decorated multi-walled carbon nanotubes modified sensor for the determination of 5-hydroxytryptophan in biological fluids, Sens. Actuators B Chem. 239 (2017) 1060–1068. https://doi.org/10.1016/j.snb.2016.08.122.
- 488 [29] X. Guo, Y. Yun, V.N. Shanov, H.B. Halsall, W.R. Heineman, Determination of Trace Metals 489 by Anodic Stripping Voltammetry Using a Carbon Nanotube Tower Electrode, 490 Electroanalysis 23 (2011) 1252–1259. https://doi.org/10.1002/elan.201000674.
- [30] W. Yue, B.L. Riehl, N. Pantelic, K.T. Schlueter, J.M. Johnson, R.A. Wilson, X. Guo, E.E.
   King, W.R. Heineman, Anodic Stripping Voltammetry of Heavy Metals on a Metal Catalyst
   Free Carbon Nanotube Electrode, Electroanalysis 24 (2012) 1039–1046.
   https://doi.org/10.1002/elan.201200065.

495

496

497

504

505

- [31] G. Liu, Y. Lin, Y. Tu, Z. Ren, Ultrasensitive voltammetric detection of trace heavy metal ions using carbon nanotube nanoelectrode array, The Analyst 130 (2005) 1098. https://doi.org/10.1039/b419447k.
- 498 [32] M.-P.N. Bui, C.A. Li, K.N. Han, X.-H. Pham, G.H. Seong, Electrochemical Determination of Cadmium and Lead on Pristine Single-walled Carbon Nanotube Electrodes, Anal. Sci. 28 (2012) 699–704. https://doi.org/10.2116/analsci.28.699.
- [33] D. Zhao, X. Guo, T. Wang, N. Alvarez, V.N. Shanov, W.R. Heineman, Simultaneous
   Detection of Heavy Metals by Anodic Stripping Voltammetry Using Carbon Nanotube
   Thread, Electroanalysis 26 (2014) 488–496. https://doi.org/10.1002/elan.201300511.
  - [34] D. Zhao, D. Siebold, N.T. Alvarez, V.N. Shanov, W.R. Heineman, Carbon Nanotube Thread Electrochemical Cell: Detection of Heavy Metals, Anal. Chem. 89 (2017) 9654–9663. https://doi.org/10.1021/acs.analchem.6b04724.
- 507 [35] J.E. Robinson, W.R. Heineman, L.B. Sagle, M. Meyyappan, J.E. Koehne, Carbon nanofiber electrode array for the detection of lead, Electrochem. Commun. 73 (2016) 89–93. https://doi.org/10.1016/j.elecom.2016.11.002.
- 510 [36] W. Cho, M. Schulz, V. Shanov, Growth termination mechanism of vertically aligned centimeter long carbon nanotube arrays, Carbon 69 (2014) 609–620. https://doi.org/10.1016/j.carbon.2013.12.088.
- 513 [37] W. Cho, M. Schulz, V. Shanov, Growth and characterization of vertically aligned centimeter long CNT arrays, Carbon 72 (2014) 264–273. https://doi.org/10.1016/j.carbon.2014.01.074.
- [38] V. Shanov, W. Cho, R. Malik, N. Alvarez, M. Haase, B. Ruff, N. Kienzle, T. Ochmann, D. Mast, M. Schulz, CVD growth, characterization and applications of carbon nanostructured materials, Surf. Coat. Technol. 230 (2013) 77–86.
  https://doi.org/10.1016/j.surfcoat.2013.06.017.
- [39] X. Guo, T. Meyung, Y. Yun, V.N. Shanov, H.B. Halsall, W.R. Heineman, Micro Solid-Contact Ion-Selective Electrode Using a Carbon Nanotube Tower as Ion-to-Electron Transducer and Conductive Substrate, Electroanalysis 24 (2012) 2045–2048. https://doi.org/10.1002/elan.201200348.
- [40] A. Doepke, C. Han, T. Back, W. Cho, D.D. Dionysiou, V. Shanov, H.B. Halsall, W.R. Heineman, Analysis of the Electrochemical Oxidation of Multiwalled Carbon Nanotube
   Tower Electrodes in Sodium Hydroxide, Electroanalysis 24 (2012) 1501–1508. 
   https://doi.org/10.1002/elan.201200105.

[41] W. Cho, M. Schulz, V. Shanov, Kinetics of Growing Centimeter Long Carbon Nanotube
 Arrays, in: S. Suzuki (Ed.), Synth. Appl. Carbon Nanotub. Their Compos., InTech, 2013.
 https://doi.org/10.5772/50837.

- [42] V.N. Shanov, A. Gorton, Y.-H. Yun, M.J. Schultz, Composite catalyst and method for manufacturing carbon nanostructured materials, WO2008105936A2, 2008. https://patents.google.com/patent/WO2008105936A2/en/enIt.pdf (accessed July 9, 2024).
- [43] Y. Yun, V. Shanov, M.J. Schulz, Z. Dong, A. Jazieh, W.R. Heineman, H.B. Halsall, D.K.Y. Wong, A. Bange, Y. Tu, S. Subramaniam, High sensitivity carbon nanotube tower electrodes, Sens. Actuators B Chem. 120 (2006) 298–304. https://doi.org/10.1016/j.snb.2006.02.030.
- [44] Q. Zhang, B. A. Calderon, C. R. Ebbing, L. J. Elston, L. W. Byrd, B.-H. Tsao, Thermal Properties Enhancement of Vertically Aligned Carbon Nanotubes-Based Metal Nanocomposites as Thermal Interface Materials, Front. Mater. 7 (2020) 572956. https://doi.org/10.3389/fmats.2020.572956.
- [45] C. Guo, C. Wang, H. Sun, D. Dai, H. Gao, A simple electrochemical sensor based on rGO/MoS2/CS modified GCE for highly sensitive detection of Pb(II) in tobacco leaves, RSC Adv. 11 (2021) 29590–29597. https://doi.org/10.1039/D1RA05350G.
- [46] H. Zhang, Y. Li, Y. Zhang, J. Wu, S. Li, L. Li, A Disposable Electrochemical Sensor for Lead Ion Detection Based on In Situ Polymerization of Conductive Polypyrrole Coating, J. Electron. Mater. 52 (2023) 1819–1828. https://doi.org/10.1007/s11664-022-10175-y.
- [47] C.E. Rahm, F. Torres-Canas, P. Gupta, P. Poulin, N.T. Alvarez, Inkjet Printed Multi-walled Carbon Nanotube Sensor for the Detection of Lead in Drinking Water, Electroanalysis 32 (2020) 1533–1545. https://doi.org/10.1002/elan.202000040.
- [48] C. Russell, P. Brandhuber, D. Lytle, Lead in Drinking Water: Past, Present, and Future, Opflow 43 (2017) 10–15. https://doi.org/10.5991/OPF.2017.43.0079.

